# Secrecy Performance Analysis of RIS-Aided Wireless Systems over Correlated Extended $\alpha$-$\eta$-$\mathcal{F}$ Composite Fading Channels

Hussien Al-Hmood, *Senior Member, IEEE,* and H. S. Al-Raweshidy, *Senior Member, IEEE*

***Abstract*—In this paper, the secrecy of the physical layer of an reconfigurable intelligent surface (RIS)-assisted wireless communications system over extended $\alpha$-$\eta$-$\mathcal{F}$ composite fading channels is analyzed. The extended $\alpha$-$\eta$-$\mathcal{F}$ composite fading model is introduced in this work as a generalization of the versatile extended $\eta$-$\mathcal{F}$ and $\alpha$-$\mu$ distributions. Accordingly, this model encompasses as special cases most of the generalized fading distributions, such as extended $\alpha$-$\eta$-$\mu$, extended $\eta$-$\mathcal{F}$, and $\alpha$-$\eta$-$\mathcal{F}$. To this effect, the probability density functions (PDFs) of a single random variable (RV) and product of two non-identically distributed variates of extended $\alpha$-$\eta$-$\mathcal{F}$ composite fading model are provided first. Thereafter, we derive mathematically tractable expressions of the average secrecy capacity (ASC), secure outage probability (SOP), lower bound of SOP (SOP$^L$), and effective secrecy throughput (EST) of RIS-assisted wireless communications system over correlated extended $\alpha$-$\eta$-$\mathcal{F}$ composite fading channels. In addition, the asymptotic expressions of the ASC, SOP, and SOP$^L$ at high average SNR regime are also presented to explain the impact of both the number of the RIS elements and fading parameters on the secrecy performance metrics. The validity of our analytical results is confirmed through Monte Carlo (MC) simulations as well as a comparison with some special cases of the extended $\alpha$-$\eta$-$\mathcal{F}$ composite fading channels.**

***Index Terms*—Average secrecy capacity, effective secrecy throughput, extended $\alpha$-$\eta$-$\mathcal{F}$ composite fading, reconfigurable intelligent surface, secure outage probability.**

## I. Introduction

RECENTLY, reconfigurable intelligent surface (RIS) has been given a special attention as a promising technology for sixth generation (6G) wireless communications systems. This is because the RIS improves the quality of the received signals via controlling the effect of the propagation environment by using passive intelligent elements [1]. Accordingly, several works have been dedicated to analyze the performance of RIS-aided the physical layer security (PLS) that leverages the physical properties of the wireless propagation medium which would lead to enhance the secrecy of the transmission in the presence of the wiretap channel [2]. For example, the authors in [3] studied the secure outage probability (SOP) over Rayleigh fading channels via applying the central limit theorem (CLT) that is widely utilized to approximate the probability density function (PDF) of the received instantaneous signal-to-noise ratio (SNR) when the number of the elements of the RIS is large. In [4], the analysis of the SOP over Rayleigh fading condition was based on assuming the RIS includes large number of elements as well as employing a Gamma distribution. This distribution was also utilized in [5] and [6] to derive the SOP of a RIS-enabled system via tightly approximating the sum of the identically distributed cascaded Rayleigh and Nakagami-$m$ fading channel coefficients, respectively. In [7], the Gamma and CLT approaches were used to provide the SOP and average secrecy rate (ASR) over Rayleigh fading channels in terms of the multivariate Fox's $H$-function FHF (mFHF). The authors of [8] analyzed the SOP and average secrecy capacity (ASC) of RIS-aided wireless network over identical Rician fading channels via employing the stochastic geometry to approximate the formulations of the PDF and CDF of the received instantaneous SNRs at the legitimate user and randomly located eavesdroppers.

To obtain better fitting to the practical measurements in comparison with the classical distributions, like Rayleigh and Nakagami-$m$, the performance indicators of RIS-assisted wireless systems were analyzed over different generalized fading channels. In particular, the secrecy performance of RIS-aided system over uncorrelated FS-$\mathcal{F}$ fading channels was studied in [9] by using a Gamma approximation approach. Conversely, the authors in [10] derived the exact and asymptotic expressions of the ASC and SOP over correlated FS-$\mathcal{F}$ fading channels via applying a copula theory to obtain the joint statistics of the Bob and Eve channels' coefficients. On the contrary of [9] and [10], the secrecy performance enhancement using a RIS technique over non-identical FS-$\mathcal{F}$ fading conditions was achieved in [11] where the performance metrics were expressed in terms of the mFHF. A mixture Gamma (MG) distribution based analysis of the ASC, ASR, and SOP of a RIS-improved PLS over unified identically distributed channel coefficients was investigated in [12].

Motivated by the observed enhancement in the performance of the PLS that is occurred via using a RIS technology [2], [11] as well as the correlation among fading parameters, the secrecy of RIS-aided communications system over correlated extended $\alpha$-$\eta$-$\mathcal{F}$ composite fading channels is analyzed in this paper. In contrast to $\alpha$ - $\mu$ fading [13], in this non-line-of-sight (NLoS) fading model, the multiple paths, shadowing, non-linearity of the propagation medium and imbalance clustering between the in-phase and quadrature (I/Q) components are simultaneously affected the received signals. This scenario can be noticed in several real-world wireless communication systems. For instance, in satellite communication systems, the signal may be reflected off the building which would lead to weak some signal paths that cause the differences in the power and number of the clusters between I/Q components. Moreover, the shadowing may occur when obstacles moving close to the receiver whereas the non-linearity of the environment may be attended due to the propagating the sound waves in the

Manuscript received June 00, 2025.

Hussien Al-Hmood is with the Electrical and Electronics Engineering Department, University of Thi-Qar, Iraq, e-mail: Hussien.Al-Hmood@utq.edu.iq. H. S. Al-Raweshidy is with the Electronic and Computer Engineering Department, Brunel University of London, UK, e-mail: Hamed.Al-Raweshidy@brunel.ac.uk.

atmosphere [14]. Consequently, the extended $\alpha$-$\eta$-$\mathcal{F}$ composite fading distribution integrates $\alpha$-$\eta$-$\mathcal{F}$ [15] and extended $\eta$-$\mathcal{F}$ [16] distributions in unified composite fading model that characterizes comprehensive propagation mediums.

The main contributions of this paper are multifold, which are summarized as follows:

- The secrecy performance of the RIS aided wireless communications systems over correlated extended $\alpha$-$\eta$-$\mathcal{F}$ composite fading channels is analyzed. To achieve this analysis, novel exact mathematically tractable PDF of the received signal envelope over extended $\alpha$-$\eta$-$\mathcal{F}$ composite fading channel is derived first. To the best of our knowledge, the extended $\alpha$-$\eta$-$\mathcal{F}$ composite fading channel model has not been yet presented in the literature.
- Providing the PDF of the product of two non-identically distributed extended $\alpha$-$\eta$-$\mathcal{F}$ composite fading variates. Moreover, general simple analytically acceptable joint PDF (JPDF) of the channel coefficients of the Bob and Eve is also given.
- Capitalizing on the above, unified expressions of the ASC, SOP, SOP$^L$, and effective secrecy throughput (EST) of RIS enabled systems are derived. Unlike [13] and [10] in which the fading channels are special cases of the extended $\alpha$-$\eta$-$\mathcal{F}$ composite fading scenario, our performance measures are derived in existence of a RIS technology and with low mathematical intricacy.
- Further insightful observations into the influence of the number of the elements of RIS and fading parameters of the channel on the performance metrics are revealed via the asymptotic behavior at high SNR values.

*Organization:* Section II explains the system and channel models are explained. Moreover, this section provides the PDF of both the single variate and product of two non-identically distributed random variables (RVs) of extended $\alpha$-$\eta$-$\mathcal{F}$ composite fading model. The exact and asymptotic expressions of the secrecy performance metrics are derived in Sections III and IV, respectively. In Section V, the numerical and simulation results are presented. Finally, Section VI highlights some conclusions about the analysis of this work.

## II. System and Channel Models

### A. System Model

In this paper, the RIS technology is employed to assist the PLS of the wireless communications system via reducing the impact of the obstacle that is located in the direct link between the Alice and Bob. In addition, the Eve is supposed to be closed to the Bob. Consequently, the coefficients of the fading channels of the Bob andEve may be correlated. Moreover, the RIS system is assumed to include $N$ elements whereas the Alice, Bob, and Eve are supposed to be equipped with a single antenna. Hence, the transmitted signal from the $n$-th element of RIS system is received by both users as explained in Fig. 1. In the same context, $\{h_{A,n}(m), h_{B,n}(m)\} \in \mathbb{C}$ with $n = 1, 2, \cdots, N$ stand for the arbitrarily distributed extended $\alpha$-$\eta$-$\mathcal{F}$ composite fading channel gains from the Alice to the $n$-th element with parameters ($\alpha_{A,n}$, $\eta_{A,n}$, $\mu_{A,n}$, $p_{A,n}$, $m_{sA,n}$, $\hat{r}_{A,n}$). For the $n$-element of the RIS to the Bob and Eve, the parameters are denoted by ($\alpha_{l,n}$, $\eta_{l,n}$, $\mu_{l,n}$, $m_{sl,n}$, $p_{l,n}$, $\hat{r}_{l,n}$) with $l \in \{B, E\}$ and $\alpha_{l,n}$, $\eta_{l,n}$, $\mu_{l,n}$, $m_{sl,n}$, and $p_{l,n}$ are the index of the non-linearity propagation environment, ratio of the powers of I/Q components, total number of the multi-path clusters, clustering imbalance between I/Q components, and shadowing severity parameter, respectively. Furthermore, $\hat{r}_{l,n}^{\alpha} = \zeta / d_{l,n}^{\sigma_{l,n}}$ is the average power of the fading envelope with $\zeta = (\lambda/4\pi)^2$ represents the near field path loss factor at a reference distance of 1 m and $\lambda$ stands for the carrier wavelength, $\sigma_{l,n}$ is the path loss exponent, and $d_{l,n}$ denotes either the RIS-B and RIS-E distances. Thus, the distance between the Bob and Eve, namely, $d_{BE}$ can be computed by the cosine law, i.e., $d_{BE}^2 = d_{B,n}^2 + d_{E,n}^2 - 2d_{B,n}d_{E,n}\cos\phi$ where $\phi$ is the angle between the RIS-B and RIS-E links [8], [17]. Besides, to achieve maximum SNR through phase shift correction, the RIS has full access to channel state information (CSI) of both links [17]. Thus, the received signal at both the Bob and Eve, $y_l(m)$ is given as [6]

$$y_l(m) = x(m) \sum_{n=1}^{N} h_{Al,n}(m) + w_l(m), \tag{1}$$

where $x(m)$ is the transmitted signal from the Alice, $h_{Al,n}(m) \triangleq h_{A,n}(m)h_{l,n}(m)$ is the total extended $\alpha$-$\eta$-$\mathcal{F}$ composite fading channel gain from the Alice to the $l$-th user through $n$-element with amplitude $|h_{Al,n}| = |h_{A,n}||h_{l,n}|$ and $w_l(m)$ is the additive white Gaussian noise (AWGN) that is assumed to have zero-mean and fixed variance.

### B. Channel Model

***Theorem** 1:* Let $\alpha$, $\eta$, $\mu$, $m_s$, $p$, $\hat{r}^{\alpha}$, $r \in \mathbb{R}^+$ where $r$ is a RV that represents the instantaneous signal power of the fading envelope, $R$, over extended $\alpha$-$\eta$-$\mathcal{F}$ composite fading channel, the PDF of $R$ is determined as

$$f_R(r) = \frac{\alpha r^{\alpha\mu-1}\left(\frac{p}{\eta}\right)^{\vartheta} {}_2F_1\left(\vartheta, \mu+m_s; \mu; -\frac{\Xi r^{\alpha}}{[r^{\alpha}/\varpi+\hat{r}^{\alpha}]}\right)}{\varpi^{\mu}\hat{r}^{-\alpha m_s}B(\mu, m_s)[r^{\alpha}/\varpi + \hat{r}^{\alpha}]^{\mu+m_s}}, \tag{2}$$

where $\Xi = (p-\eta)/\eta\varpi$, $\vartheta = \mu p/(1+p)$, In addition, $\hat{r}^{\alpha} = \mathsf{E}[R^{\alpha}]$ is the average power of the fading envelope with $\mathsf{E}[.]$ stands for the expectation operator, ${}_2F_1(.;.;.)$ represents the generalized Gauss hypergeometric function [18, eq. (1.4.1)] and $B(.,.)$ denotes the Beta function [18, eq. (1.1.43)] and

$$\varpi = \left(\frac{B(\mu, m_s)\left(\frac{\eta}{p}\right)^{\vartheta}}{B(\mu+\frac{2}{\alpha}, m_s-\frac{2}{\alpha}){}_2F_1\left(\vartheta, \mu+\frac{2}{\alpha}; \mu; \frac{\eta-p}{\eta}\right)}\right)^{\frac{\alpha}{2}}, \tag{3}$$

with $m_s > 2/\alpha$.

*Proof:* See Appendix A.A. ∎

It is interesting to mention that the extended $\alpha$-$\eta$-$\mathcal{F}$ composite fading channel encompasses several generalized fading models as special cases as shown in Table I. From this table, when $p = 1$, our proposed fading model becomes the $\alpha$-$\eta$-$\mathcal{F}$ composite fading condition [15]. Accordingly, the conventional distributions, namely, Rayleigh and Nakagami-$m$ are also considered as special scenarios of the extended $\alpha$-$\eta$-$\mathcal{F}$ composite fading model. However, in the extended $\alpha$-$\eta$-$\mathcal{F}$ composite fading, the number of the clusters of the in-phase and quadrature components are different. Additionally,

This article has been accepted for publication in a future issue of this journal, but has not been fully edited. Content may change prior to final publication.
Citation information: DOI: 10.1109/TVT.2026.3655009,



$$f_{\Lambda}(r)=\alpha_1\sum_{n_1,n_2=0}^{\infty}\frac{\Delta_{n_1,n_2}\varpi_1^{-\mu_1}r^{u_{n_1}-1}}{\varpi_2^{u_{n_1}/\alpha_2-n_2}(\hat{r}_1\hat{r}_2)^{u_{n_1}}}H_{2,2}^{2,2}\left[\frac{\varpi_2^{-\frac{\alpha_1}{\alpha_2}}r^{\alpha_1}}{\varpi_1(\hat{r}_1\hat{r}_2)^{\alpha_1}}\middle|\begin{matrix}(1-m_{s_2}-u_{n_1}/\alpha_2,\alpha_1/\alpha_2),(1-\mu_1-m_{s_1}-n_1,1)\\(0,1),(-u_{n_1}/\alpha_2+\mu_2+n_2,\alpha_1/\alpha_2)\end{matrix}\right]. \quad (4)$$

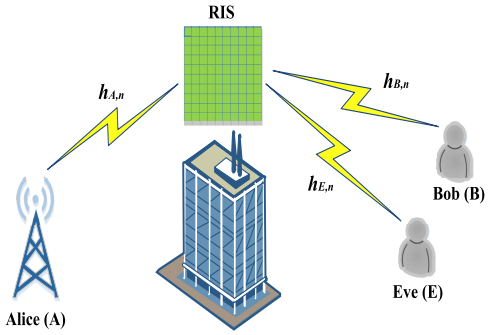


Fig. 1. System model of RIS-aided system in presence of the eavesdropper.

TABLE I
SPECIAL CASES OF THE EXTENDED $\alpha$-$\eta$-$\mathcal{F}$ COMPOSITE FADING MODEL.

| Fading Models | Parameters of Extended $\alpha$-$\eta$-$\mathcal{F}$ Fading |
|---|---|
| $\eta$-$\mu$/IG [19] | $\underline{p}=1$, $\underline{\alpha}=2$, $\underline{\eta}=\eta$, $\underline{\mu}=\mu$, $\underline{m_s}=m_s$ |
| FS-$\mathcal{F}$ [20] | $\underline{p}=\eta$, $\underline{\alpha}=2$, $\underline{\eta}=p$, $\underline{\mu}=m$, $\underline{m_s}=m_s$ |
| Extended $\eta$-$\mathcal{F}$ [16] | $\underline{p}=p$, $\underline{\alpha}=2$, $\underline{\eta}=\eta$, $\underline{\mu}=m$, $\underline{m_s}=m_s$ |
| Extended $\eta$-$\mu$ [21] | $\underline{p}=p$, $\underline{\alpha}=2$, $\underline{\eta}=\eta$, $\underline{\mu}=\mu$, $\underline{m_s}\to\infty$ |
| $\alpha$-$\mathcal{F}$ [22] | $\underline{p}=\eta$, $\underline{\alpha}=\alpha$, $\underline{\eta}=p$, $\underline{\mu}=\mu$, $\underline{m_s}=m_s$ |
| $\alpha$-$\mu$ [13] | $\underline{p}=\eta$, $\underline{\alpha}=\alpha$, $\underline{\eta}=p$, $\underline{\mu}=\mu$, $\underline{m_s}\to\infty$ |
| $\alpha$-$\eta$-$\mathcal{F}$ [15] | $\underline{p}=1$, $\underline{\alpha}=\alpha$, $\underline{\eta}=\eta$, $\underline{\mu}=m$, $\underline{m_s}=m_s$ |
| Extended $\alpha$-$\eta$-$\mu$ [23] | $\underline{p}=p$, $\underline{\alpha}=\alpha$, $\underline{\eta}=\eta$, $\underline{\mu}=\mu$, $\underline{m_s}\to\infty$ |
| Extended $\alpha$-$\mathcal{F}$ | $\underline{p}=p$, $\underline{\alpha}=\alpha$, $\underline{\eta}=1$, $\underline{\mu}=m$, $\underline{m_s}=m_s$ |

the impacts of both the shadowing and non-linearity of the propagation medium are taken into account.

### C. PDF of the Product of Two Non-Identically Distributed Extended $\alpha$-$\eta$-$\mathcal{F}$ Composite RVs

***Theorem** 2:* For two arbitrarily distributed extended $\alpha$-$\eta$-$\mathcal{F}$ RVs $R_1$ and $R_2$ with parameters ($\alpha_1$, $\eta_1$, $\mu_1$, $m_{s_1}$, $p_1$, $\hat{r}_1$) and ($\alpha_2$, $\eta_2$, $\mu_2$, $m_{s_2}$, $p_2$, $\hat{r}_2$), respectively, the PDF of $\Lambda=R_1R_2$ is obtained in (4) that is presented at the top of this page. In (4), $u_{n_i}=\alpha_i(\mu_i+n_i)$ for $i=1,2$, $(.)_n$ is the Pochhammer symbol [18, eq. (1.1.53)], $H_{c,d}^{a,b}[.]$ is the univariate FHF [18 , eq. (1.5.15)], and

$$\Delta_{n_1,n_2}=\prod_{i=1}^{2}\frac{(\vartheta_i)_{n_i}(-\Xi_i)^{n_i}\left(\frac{p_i}{\eta_i}\right)^{\vartheta_i}}{\Gamma(\mu_i)\Gamma(m_{s_i})(\mu_i)_{n_i}n_i!}. \quad (5)$$

*Proof:* See Appendix A.B. ■

***Lemma** 1:* The expected value of $\Lambda$ to power $k$ is derived as

$$\mathsf{E}[\Lambda^k]=\prod_{i=1}^{2}\Phi_i(k), \quad (6)$$

where

$$\Phi_i(k)=\frac{B\left(\mu_i+\frac{k}{\alpha_i},m_{s_i}-\frac{k}{\alpha_i}\right){}_2F_1\left(\vartheta_i,\mu_i+\frac{k}{\alpha_i};\mu_i;-\varpi_i\Xi_i\right)}{B(\mu_i,m_{s_i})\left(\frac{p_i}{\eta_i}\right)^{-\vartheta_i}\varpi_i^{-\frac{k}{\alpha_i}}\hat{r}_i^{-k}}. \quad (7)$$

*Proof:* See Appendix A.C. ■

### D. RIS-Aided PLS over Correlated Composite Extended $\alpha$-$\eta$-$\mathcal{F}$ Fading Channels

According to (1), it can be noticed that the PDF of $|h_{Al,n}|$ can be deduced via recalling the result of Theorem 2, i.e., $f_{|h_{Al,n}|}(r)=f_{\Lambda}(r)$. Furthermore, the sum of $|h_{Al,n}|$ of all elements of RIS, namely, $|h_l|=\sum_{n=1}^{N}|h_{Al,n}|$, provides the total amplitude of the channel gain from the Alice to the $l$-th user. Therefore, based on (6), the PDF of the sum of i.n.d. of $|h_{Al,n}|$ are required. However, the PDF of $|h_{Al,n}|$ may be expressed in terms of the double infinite series and FHF. Thus, to avoid the multiple infinite series and mFHF expressions of the PDF of $|h_l|$ as well as due to the proximity of the Eve from the Bob, all the cascaded channel gains $|h_{Al,n}|$ are assumed to be identically distributed[1]. Also, to overcome the aforementioned mathematical challenges, the first term of a Laguerre expansion [24] is employed to approximate with high accuracy the distribution of $|h_l|$ for the exponential model. This approximation would lead to obtain the performance metrics in simple analytically tractable expressions. Hence, the PDF of $\gamma$ is expressed as [10, eq. (5)]

$$f_l(\gamma)\approx\frac{\gamma^{\frac{a_l-1}{2}}}{2b_l^{a_l+1}\Gamma(a_l+1)\bar{\gamma}_l^{\frac{1+a_l}{2}}}e^{-\frac{\sqrt{\gamma}}{b_l\sqrt{\bar{\gamma}_l}}}, \quad (8)$$

where the parameters $a_l$ and $b_l$ are computed by

$$a_l=\frac{N\mathsf{E}\left[|h_{Al}|\right]^2}{\mathsf{E}\left[|h_{Al}|^2\right]-\mathsf{E}\left[|h_{Al}|\right]^2}-1, \quad \text{and} \quad b_l=\frac{N\mathsf{E}\left[|h_{Al}|\right]}{a_l+1}, \quad (9)$$

with

$$\mathsf{E}\left[|h_{Al}|^k\right]\overset{(t_1)}{=}\Phi_A(k)\Phi_l(k), \quad (10)$$

where $(t_1)$ obtains with the aid of (6) and $\Phi_l(k)$ for $l\in\{B,E\}$ are provided in (7).

[1]Without loss of generality, we have used $|h_l|=N|h_{Al}|$ where $|h_{Al}|=|h_{Al,n}|$ and $(\alpha_l,\eta_l,\mu_l,m_{sl},p_l,\hat{r}_l)=(\alpha_{l,n},\eta_{l,n},\mu_{l,n},m_{sl,n},p_{l,n},\hat{r}_{l,n})$ for $n=1,\cdots,N$ and $l\in\{A,B\}$.

This article has been accepted for publication in a future issue of this journal, but has not been fully edited. Content may change prior to final publication.
Citation information: DOI: 10.1109/TVT.2026.3655009,



$$P_c = \frac{\Psi\sqrt{\frac{\theta^a}{\theta-1}}}{2}\sum_{n=0}^{\infty}\frac{\left(\frac{1}{\Upsilon_E}\sqrt{1-\frac{1}{\theta}}\right)^{\psi_n}\rho^n}{(a+1)_n n!}H_{0,1:2,2;1,1}^{1,0:2,0;1,1}\left[\frac{\sqrt{\theta-1}}{\Upsilon_B},\frac{\sqrt{\theta-1}}{\sqrt{\theta}\Upsilon_E}\middle|\begin{matrix}-:(1,1);-;(-\frac{1+\psi_n}{2},\frac{1}{2})\\(-\frac{\psi_n}{2};\frac{1}{2},\frac{1}{2}):(\psi_n,1),(0,1);(0,1),(0,1)\end{matrix}\right]. \quad (19)$$

For correlated fading channels $|h_B|$ and $|h_E|$ that have the PDF given in (8), the JPDF is written as

$$f(\gamma_B,\gamma_E)\overset{(t_2)}{=}\frac{(1-\rho)^{a+1}}{4\Gamma(a+1)\rho^{\frac{a}{2}}(\Upsilon_B\Upsilon_E)^{\frac{a}{2}+1}}\gamma_B^{\frac{a-2}{4}}\gamma_E^{\frac{a-2}{4}} \times\exp\left(-\left(\frac{\sqrt{\gamma_B}}{\Upsilon_B}+\frac{\sqrt{\gamma_E}}{\Upsilon_E}\right)\right)I_a\left(2\sqrt{\frac{\rho\sqrt{\gamma_B\gamma_E}}{\Upsilon_B\Upsilon_E}}\right), \quad (11)$$

where $(t_2)$ follows [25, eq. (28)] after applying a suitable change of the variables, $a=a_l$ and $\Upsilon_l=(1-\rho)b_l\sqrt{\gamma_l}$ with $l\in\{B,E\}$, $\gamma_B$ and $\gamma_E$ are the instantaneous SNR at the Bob and Eve, respectively. Moreover, $0\le\rho<1$ represents the correlation coefficient with $\rho=0$ stands for uncorrelated fading channels and $I_a(.)$ is the modified Bessel function of the first kind of the order $a$ [18, eq. (1.4.12)].

***Lemma** 2:* It is worthy to mention that the function $I_a(.)$ of (11) is expressed in terms of an infinite series in this work. Hence, the derived expressions of the secrecy performance metrics are written in terms of an infinite series. Consequently, this series should be truncated for a certain number of terms, $M$, that satisfies the required figure of accuracy with the truncation error, $\varepsilon(M)$, which is expressed as

$$\varepsilon(M)=1-(1-\rho)^{a+1}\sum_{n=0}^{M}\rho^n\frac{(1+a)_n}{n!}. \quad (12)$$

*Proof:* See Appendix A.D. ■

## III. Exact Secrecy Performance Analysis

In this section, the secrecy performance metrics of RIS-enabled system over correlated extended $\alpha$-$\eta$-$\mathcal{F}$ composite fading channels are provided. In particular, tractable expressions of the ASC, SOP, SOP$^L$, and EST are derived.

### A. ASC

The ASC is an important performance metric that measures the average of the instantaneous secrecy capacity $C_s(\gamma_B,\gamma_E)=C_B-C_E$ in which $C_B$ and $C_E$ indicate the capacity of the Bob and Eve, respectively. In other words, the ASC can be calculated by [26, eq. (17)]

$$\bar{C}_s=\int_0^{\infty}\int_0^{\gamma_B}\log_2\left(\frac{1+\gamma_B}{1+\gamma_E}\right)f(\gamma_B,\gamma_E)d\gamma_E d\gamma_B \quad (13)$$

where $f(\gamma_B,\gamma_E)$ is the JPDF of $\gamma_B$ and $\gamma_E$,

*Corollary 1:* The ASC over correlated fading channels can be evaluated by

$$\bar{C}_s=\frac{\Psi}{\ln(2)}\sum_{n=0}^{\infty}\frac{\left(\frac{\Upsilon_B}{\Upsilon_E}\right)^{\psi_n}\rho^n}{(a+1)_n n!}(J_1'-J_2'), \quad (14)$$

where $\Psi=(1-\rho)^{a+1}/\Gamma^2(1+a)$, $\psi_n=a+n+1$ whereas $J_1'$ and $J_2'$ are respectively expressed by

$$J_1'=H_{1,0:2,2;1,2}^{0,1:1,2;1,1}\left[\Upsilon_B^2,\frac{\Upsilon_B}{\Upsilon_E}\middle|\begin{matrix}(1-2\psi_n;2,1):\\-:\\(1,1),(1,1);(1-\psi_n,1)\\(1,1),(0,1);(0,1),(-\psi_n,1)\end{matrix}\right], \quad (15)$$

and

$$J_2'=H_{2,1:2,2;0,1}^{0,2:1,2;1,0}\left[\Upsilon_B^2,\frac{\Upsilon_B}{\Upsilon_E}\middle|\begin{matrix}(1-2\psi_n;2,1)\\(-\psi_n;2,1):\\,(1-\psi_n;2,1):(1,1),(1,1);-\\(1,1),(0,1);(0,1)\end{matrix}\right], \quad (16)$$

where $H_{a_2,b_2:c_2,d_2;e_2,f_2}^{a_1,b_1:c_1,d_1;e_1,f_1}[.]$ is the bivariate FHF (BFHF) [27, eq. (2.57)].

Although (14) is novel, its expressed in terms of the BFHF which is a result of the interactions of different factors that are related to intricacy of the fading channel. Thus, this expression does not give clear insights about the impact of the channel parameters and RIS technology on the system behavior. Accordingly, to cope this challenge, the asymptotic expressions at high average SNR are derived in the next section via employing the result of Corollary 1.

*Proof:* See Appendix B.A. ■

### B. SOP

The SOP is introduced as the probability of reducing the instantaneous secrecy capacity, $C_s(\gamma_B,\gamma_E)$, to less than the target secrecy threshold value, $R_s$, i.e., $Pr\{C_s(\gamma_B,\gamma_E)<R_s\}$. Hence, the SOP can be computed by [26, eq. (23)]

$$\text{SOP}=1-P_c, \quad (17)$$

where $P_c$ is the complementary secrecy outage probability (CSOP) and computed by [26, eq. (24)]

$$P_c=\int_0^{\infty}\int_{\theta\gamma_E+\theta-1}^{\infty}f(\gamma_B,\gamma_E)d\gamma_B\gamma_E, \quad (18)$$

with $\theta=\exp(R_s)\ge 1$.

*Corollary 2:* The $P_c$ over correlated fading channels is provided in (19) shown at the top of this page.

*Proof:* See Appendix B.B. ■

### C. SOP$^L$

The SOP$^L$ can be deduced from (17) via inserting $\gamma_E\to\infty$ in (18) as follows

$$\text{SOP}^L=1-P_c^L, \quad (20)$$

with

$$P_c^L=\int_0^{\infty}\int_{\theta\gamma_E}^{\infty}f(\gamma_B,\gamma_E)d\gamma_B\gamma_E. \quad (21)$$

This article has been accepted for publication in a future issue of this journal, but has not been fully edited. Content may change prior to final publication.
Citation information: DOI: 10.1109/TVT.2026.3655009,



$$P_c^{\text{Asy}} \simeq \frac{\Psi(\sqrt{\theta-1})^a}{2\sqrt{\theta}\Upsilon_E^{a+1}} \sum_{n=0}^{\infty} \frac{\rho^n}{(a+1)_n n!} \left(\frac{\sqrt{\theta-1}}{\Upsilon_E\sqrt{\theta}}\right)^n \left\{\Gamma(\psi_n)\left\{\Gamma\left(\frac{\psi_n}{2}\right)\Gamma\left(-\frac{\psi_n}{2}\right) + \Gamma(\psi_n)\left(\frac{\theta\Upsilon_E}{\sqrt{\theta-1}}\right)^{\psi_n}\right\}\right.$$
$$\left. - \frac{1}{\psi_n}\left(\frac{\sqrt{\theta-1}}{\Upsilon_B}\right)^{\psi_n}\left\{\frac{\Gamma(-\psi_n)\Gamma\left(\frac{\psi_n}{2}\right)}{\Gamma\left(-\frac{\psi_n}{2}\right)} + \Gamma(2\psi_n)\left(\frac{\theta\Upsilon_E}{\sqrt{\theta-1}}\right)^{2\psi_n}\right\}\right\}. \quad (27)$$

*Corollary 3:* The SOP$^L$ over correlated fading channels is obtained as

$$P_c^L = \Psi \sum_{n=0}^{\infty} \frac{\rho^n}{(1+a)_n n!} H_{2,2}^{2,1}\left[\frac{\sqrt{\theta}\Upsilon_E}{\Upsilon_B}\middle|\begin{matrix}(1-\psi_n,1),(1,1)\\(\psi_n,1),(0,1)\end{matrix}\right]. \quad (22)$$

*Proof:* See Appendix B.C. ∎

### D. EST

The EST is an important behavior metric that obviously includes the constraints of both the reliability and secrecy of the tapping channel. It basically measures the rate of the average secure information that is transmitted from the Alice to the Bob in absence of the Eve. Mathematically, the EST can be written as [28, eq. (60)]

$$\text{EST} = R_s(1 - \text{SOP}). \quad (23)$$

Combining (17) and (19) alongside with (23), the result is the EST over correlated fading channels.

## IV. Asymptotic Secrecy Performance Analysis

In this section, similar to [13], the asymptotic expressions of the ASC, SOP, and SOP$^L$ when $\bar{\gamma}_B$ and $\bar{\gamma}_B$ tend to $\infty$ are given. These expressions can be used to earn further insightful onto the impact of the fading parameters on the secrecy behavior of the system.

### A. Asymptotic ASC

*Corollary 4:* The asymptotic expression of the ASC at $\bar{\gamma}_l \to \infty$ with $l \in \{B, E\}$, $\bar{C}_s^{\text{Asy}}$, is expressed as

$$\bar{C}_s^{\text{Asy}} \simeq \frac{\Psi}{\ln(2)} \sum_{n=0}^{\infty} \frac{\left(\frac{\Upsilon_B}{\Upsilon_E}\right)^{\psi_n}\rho^n}{(a+1)_n n!}(J_1'^{\text{Asy}} - J_2'^{\text{Asy}}), \quad (24)$$

where

$$J_1'^{\text{Asy}} = \Theta_n - \frac{1}{\psi_n\Upsilon_B^{2\psi_n}}\left\{\Gamma(\psi_n)\Gamma(-\psi_n) + \frac{\Gamma(2\psi_n)\Upsilon_E^{2\psi_n}}{\Gamma(1-2\psi_n)}\right\}, \quad (25)$$

and

$$J_2'^{\text{Asy}} = \Theta_n - \frac{\Gamma(\psi_n)\Gamma(-\frac{\psi_n}{2})}{\Upsilon_B^{\psi_n}}\left\{\Gamma\left(\frac{\psi_n}{2}\right) + \frac{\Gamma(1+\psi_n)}{2}\Upsilon_E^{2\psi_n}\right\}, \quad (27)$$

with $\Theta_n = \Gamma^2(\psi_n)\left(\frac{\Upsilon_E}{\Upsilon_B}\right)^{\psi_n}$.

*Proof:* See Appendix C.A. ∎

### B. Asymptotic SOP

*Corollary 5:* When $\bar{\gamma}_B$ and $\bar{\gamma}_E$ go to $\infty$, the asymptotic of the CSOP that is given in (19), $P_c^{Asy}$, is derived as in (27) provided at the top of this page.

*Proof:* See Appendix C.B. ∎

### C. Asymptotic SOP$^L$

*Corollary 6:* The expression of SOP$^{L,\text{Asy}}$ when both $\bar{\gamma}_B$ and $\bar{\gamma}_E$ approach $\infty$ is obtained as

$$\text{SOP}^{L,\text{Asy}} \simeq 1 - \Psi \sum_{n=0}^{\infty} \frac{\rho^n}{(1+a)_n n!} \times \left\{\Gamma^2(\psi_n) - \frac{\Gamma(2\psi_n)}{\psi_n}\left(\frac{\sqrt{\theta}\Upsilon_E}{\Upsilon_B}\right)^{\psi_n}\right\}. \quad (28)$$

*Proof:* See Appendix C.C. ∎

## V. Numerical and Simulation Results

In this section, the influences of the parameters $\alpha$, $\eta$, $\mu$, $m_s$, and $p$ of the correlated extended $\alpha$-$\eta$-$\mathcal{F}$ composite fading channels on the secrecy performance metrics of RIS-aided wireless communications systems are explained. Furthermore, the impacts of the correlation coefficient, $\rho$, number of the elements of a RIS technique, $N$, as well as the distance between the Bob and Eve, $d_{BE}$, and angle $\phi$ are also analyzed. The accuracy of the analytical results is verified through the Monte-Carlo simulations where the former are represented by the markers whereas the latter are demonstrated by the solid lines [2]. Further validations of the correctness of our derived expressions have been performed via the comparison with the results of some previous works as well as special cases of the extended $\alpha$-$\eta$-$\mathcal{F}$ composite fading channels that are illustrated in Table 1. Additionally, the asymptotic behaviors at high average SNR are depicted by the dashed lines[3]. Besides, the fading parameters of each link are set to ($\alpha_l$, $\eta_l$, $m_{s_l}$, $p_l$) = (1.5, 2, 2.5, 0.1) for $l \in \{A, B, E\}$, $\mu_A$ = 1.5, $\mu_B$ = $\mu_E$ = 2.5, $d_{BE} = 15$ m, $\phi = 70°$, $d_{E,n} = 15$ $m$ and $\sigma = 2$. Moreover, in all our results, the number of terms of the infinite series, $M$, is chosen to be 25 which is sufficient to achieve $\varepsilon(M) \leq 10^{-6}$ via using (12).

Fig. 2 illustrates the ASC versus $\lambda = \bar{\gamma}_B/\bar{\gamma}_E$ for $\rho = 0.1$, $\bar{\gamma}_E = 0$ dB and different $m_s$ and $N$. In this figure, the cases of light, moderate, and heavy shadowing that are represented

[2]In this work, the results are evaluated via developing the MATLAB code that is presented in: https://github.com/hugerles/extended.git. Additionally, the BFHF has been numerically calculated by the code of [29].

[3]Due to the linear relation between the two formats of the extended $\alpha$-$\eta$-$\mathcal{F}$ composite fading channels via $\eta_1 = (1+\eta_2)/(1-\eta_2)$ and $p_1 = (1+p_2)/(1-p_2)$ [23], all the curves are plotted by using Format 1.

This article has been accepted for publication in a future issue of this journal, but has not been fully edited. Content may change prior to final publication.
Citation information: DOI: 10.1109/TVT.2026.3655009,



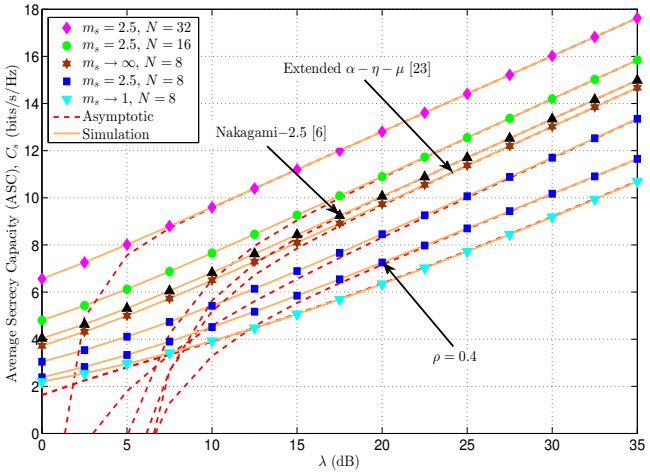


Fig. 2. ASC versus $\lambda$ for $d_{BE} = 15$ m, $\phi = 70°$, $\sigma = 2$, $\alpha = 1.5$ and different $m_s$ and $N$.

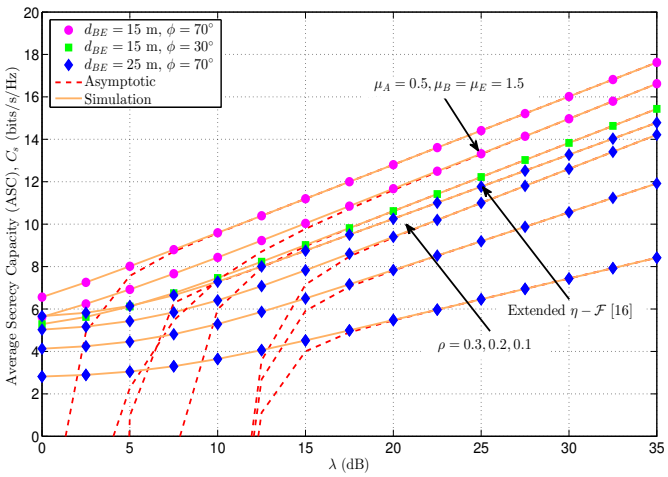


Fig. 3. ASC versus $\lambda$ for $m_{s_A} = 1.5$, $m_{s_B} = m_{s_E} = 2.5$, $N = 32$, $\sigma = 2$ and different $d_{BE}$, $\phi$, $\mu$, and $\rho$.

by $m_s \to \infty$, $m_s = 2.5$, and $m_s \to 1$, respectively, are studied. From Fig. 2, it can be noticed that the ASC improves when $m_s$ and/or $N$ increase. This is due to the fact that as $m_s$ increases, the shadowing impact on the received signal of the Bob becomes low whereas the phase error of this signal decreases with the increasing in $N$. For instance, at constant $\lambda = 25$ dB and $N = 8$, the values of ASC are 7.72 and 10.07 for $m_s \to 1$ and $m_s = 2.5$, respectively. In the same context, when $N$ changes from 8 to 16 and 32, the ASC enhances by roughly $24.63\%$ and $43.09\%$, respectively. In Fig. 2, it can also be observed that the ASC decreases with the increasing in the correlation coefficient, $\rho$. This refers to the high similarity in the behavior of both the channels of the Bob and Eve which would reduce the likelihood of achieving the target secrecy rate by the transmitter. For example, at fixed $\lambda = 20$ dB, $m_s = 2.5$, $N = 8$, the ASC falls by nearly $14.20\%$ when $\rho$ rises from 0.1 to 0.4. The ASC of correlated extended $\alpha$-$\eta$-$\mu$ fading channels is also showed in Fig. 2 by inserting $m_s \to \infty$ in (14) and (24). In addition, the ASC when the links of both the Bob and Eve undergo Nakagami-2.5 fading channel [6] that is obtained via substituting $\alpha = 2$, $\eta = p = 2$, $m_s \to \infty$, $\mu_A = 1.5$, and $\mu_B = \mu_E = 2.5$ is also provided in Fig. 2. Accordingly, $\alpha$, $p$, and $m_s \to \infty$ of Nakagami-2.5 fading model are higher than that of the extended $\alpha$-$\eta$-$\mathcal{F}$ composite fading channel. Hence, Nakagami-2.5 outperforms both the extended $\alpha$-$\eta$-$\mu$ and extended $\alpha$-$\eta$-$\mathcal{F}$ composite fading channels in terms of the ASC as demonstrated in Fig. 2.

Fig. 3 shows the ASC against $\lambda$ for $N = 32$, $\bar{\gamma}_E = 0$ dB and various values of $d_{BE}$, $\phi$ and $\rho$ for the case of $d_{BE} = 25$ m and $\phi = 70°$. As anticipated, the ASC fairly reduces as $d_{BE}$ increases and/or $\phi$ decreases. This is because the distance between the Bob and RIS, $d_{B,n}$ becomes long in both scenarios. In other words, the Bob moves away the RIS. For example, at $\lambda = 25$ dB and fixed $\phi = 70°$, the ASC drops by approximately $23.66\%$ when $d_{BE}$ changes from 15 m to 25 m. Moreover, at the same $\lambda$ and constant $d_{BE}$ at 15 m, the variation in $\phi$ from 70° to 30° would lead to drop the ASC by roughly $9.98\%$. Similar to Fig. 2, Fig. 3 demonstrates that the

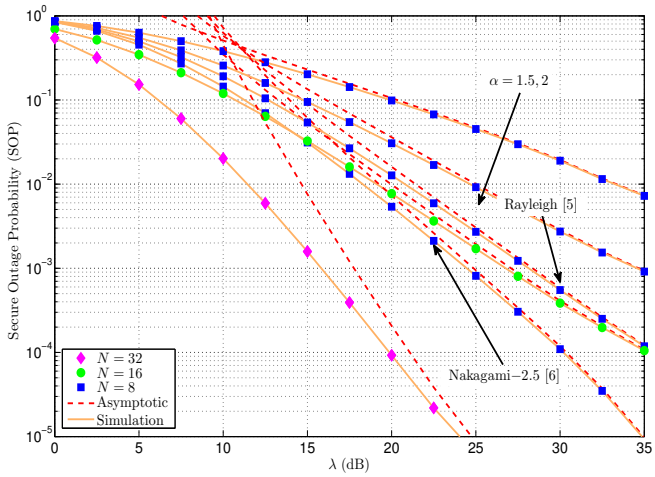


Fig. 4. SOP versus $\lambda$ for $d_{BE} = 15$ m, $\phi = 70°$, $\sigma = 2$, $\rho = 0.25$, $R_s = 1$ and different $N$ and $\alpha$.

degradation in $\rho$ enhances the ASC. In addition, the decreasing in $\mu$ would reduce the ASC, as anticipated. The reason refers to the low number of the signal paths that reaches to the receiver side which is consistent with [30]. Fig. 3 also includes the ASC over extended $\eta$-$\mathcal{F}$ composite fading condition in which $\alpha = 2$ whereas in extended $\alpha$-$\eta$-$\mathcal{F}$ composite fading model, $\alpha = 1.5$. Consequently, the increasing in $\alpha$ would improve the secrecy performance of the system.

Figs. 4 and 5 respectively depict the SOP and SOP$^L$ versus $\lambda$ for $\bar{\gamma}_E = -10$ dB and various $N$. Furthermore, a comparison with some fading models that are special cases of correlated extended $\alpha$-$\eta$-$\mathcal{F}$ composite fading channels is carried out in these figures. From both figures, one can see that both the SOP and SOP$^L$ degrades when $N$ increases and/or $\rho$ decreases. This is because the high increasing in the instantaneous capacity of the Bob in a comparison with the Eve as its demonstrated in the analysis of Figs. 2 and 3. For instance, when $\lambda$ is fixed at 15 dB and $N$ changes from 16 to 32, the SOP and SOP$^L$ are decreased by approximately $95.14\%$ and $93.08\%$, respectively. Additionally, as $\alpha$ increases from 1.5 to 2, the SOP decreases

This article has been accepted for publication in a future issue of this journal, but has not been fully edited. Content may change prior to final publication.
Citation information: DOI: 10.1109/TVT.2026.3655009,



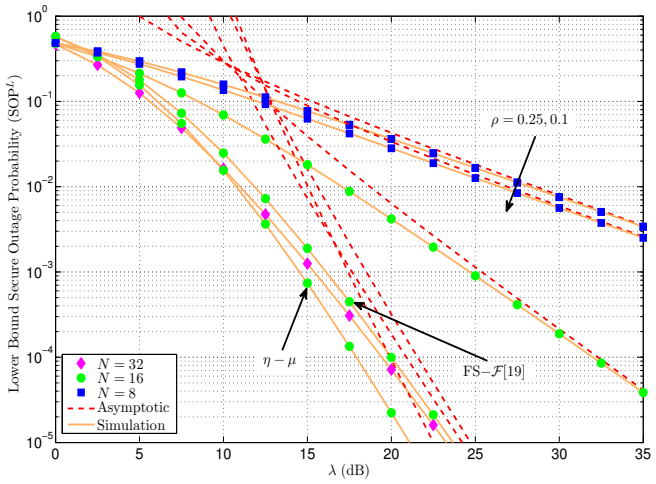


Fig. 5. SOP$^L$ versus $\lambda$ for $d_{BE} = 15$ m, $\phi = 70°$, $\sigma = 2$, $\alpha = 1.5$, $R_s = 1$ and different $N$ and $\rho$.

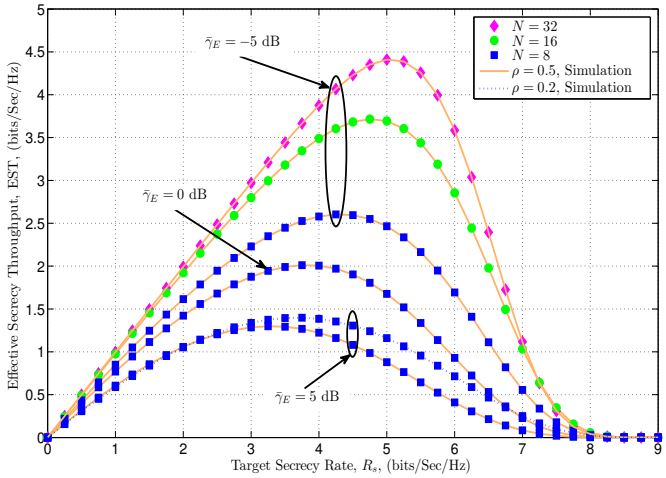


Fig. 6. EST versus $R_s$ for different $\bar{\gamma}_E$, $N$ and and $\rho$.

from $20.22 \times 10^{-2}$ to $9.48 \times 10^{-2}$. Furthermore, the SOP$^L$ for $\rho = 0.25$ is $7.73 \times 10^{-2}$ whilst its value for $\rho = 0.1$ is $6.26 \times 10^{-2}$. From Figs. 4 and 5, it can be observed that the SOP$^L$ is always less than the corresponding SOP which is consistent with the results of [30, eq. (20)]. Besides, Fig. 4 encompasses the SOP when the links are subject to Nakagami-2.5 [6] and Rayleigh [5] fading channels. As expected, Nakagami-2.5 has lower SOP than Rayleigh due to the increasing in $\mu$ from 1 to 2.5. Moreover, Fig. 5 also explains the SOP$^L$ of correlated FS-$\mathcal{F}$ [10] fading channel and $\eta$ - $\mu$ fading scenario that has not been yet reported by previous works.

The adherence between the numerical and simulation curves can be perceived in all cases of the proposed scenarios. Also, the asymptotic behaviors of Figs. 2-5 follow their analytical counterparts at high $\bar{\gamma}_B$.

Fig. 6 portrays the EST versus $R_s$ for different $N$, $\rho$, $\bar{\gamma}_E$, and $\bar{\gamma}_B = 10$ dB. In all cases, it can be noticed that the curve of the EST has a convex shape. In other words, the EST rises to a specific $R_s$ and then drops afterward. To achieve lower $R_s$, few security resources are required which would increase the EST. Conversely, a higher $R_s$ needs more resources which would exacerbate the channel impairments that reduce the EST. In the same figure, when $N$ increases, $\bar{\gamma}_E$ decreases, or/and $\rho$ drops at constant $R_s$, the EST becomes high and for the same reasons that have been explained for Figs. 4 and 5.

## VI. Conclusion

The secrecy performance of RIS-enabled communications system over correlated extended $\alpha$-$\eta$-$\mathcal{F}$ composite fading channels was analyzed in this article. The exact expressions of the PDF of both the signal envelope of single RV and product of two i.n.d. extended $\alpha$-$\eta$-$\mathcal{F}$ composite variates were provided. Thereafter, the metrics ASC, SOP, SOP$^L$, and EST of RIS-assisted PLS over correlated extended $\alpha$-$\eta$-$\mathcal{F}$ composite fading channels was accurately analyzed. Further insights about the impact of the fading parameters as well as the number of the elements of a RIS technology were deduced via the asymptotic behavior of the ASC, SOP, and SOP$^L$ at high average SNR values of the Bob and Eve. The results showed that the PLS improves when the number of the elements of RIS increases or/and the correlation coefficient decreases. The behaviors of the secrecy performance metrics of some special cases of extended $\alpha$-$\eta$-$\mathcal{F}$ composite fading channels were also presented. Hence, the derived expressions can be employed for different generalized composite fading models that have not been yet reported in the technical literature.

## Appendix A

### A. Proof of Theorem 1

The envelope of the extended $\alpha$-$\eta$-$\mathcal{F}$ composite fading distribution, $R$, is expressed as

$$R^{\alpha} = \sum_{i=1}^{\mu_x} \mathcal{A}^2 X_i^2 + \sum_{j=1}^{\mu_y} \mathcal{A}^2 Y_j^2, \tag{29}$$

where $\mathcal{A}$ is the inverse Nakagami-$m$ RV, $X_i^2$ stand for the in-phase components of the cluster $i$ with number of multipath clusters $\mu_x$ and $Y_j^2$ denote the quadrature components of the cluster $j$ with number of clusters $\mu_y$. Additionally, $X_i^2$ and $Y_j^2$ are mutually independent Gaussian variates with zero mean, i.e., $\mathsf{E}[X_i] = \mathsf{E}[Y_j]$.

On the other side, the received signal envelope over extended $\eta$-$\mathcal{F}$ composite fading, $R_{E,\eta-\mathcal{F}}$, is given as [16]

$$R_{E,\eta-\mathcal{F}}^2 = \sum_{i=1}^{\mu_x} \mathcal{A}^2 X_i^2 + \sum_{j=1}^{\mu_y} \mathcal{A}^2 Y_j^2. \tag{30}$$

From (29) with (30), it can be noted that

$$R^{\alpha} = R_{E,\eta-\mathcal{F}}^2. \tag{31}$$

Now, let us consider

$$Z_{E,\eta-\mathcal{F}} = R_{E,\eta-\mathcal{F}}^2. \tag{32}$$

Using the change of the variate of (32) in [16, eq. (4)], we

This article has been accepted for publication in a future issue of this journal, but has not been fully edited. Content may change prior to final publication.
Citation information: DOI: 10.1109/TVT.2026.3655009,



$$f_{\Lambda}(r)=\sum_{n_1,n_2=0}^{\infty}\left(\prod_{i=1}^{2}\frac{\alpha_i}{\varpi_i^{\mu_i}\hat{r}_i^{u_{n_i}}}\right)\frac{\Delta_{n_1,n_2}}{r^{1-u_{n_2}}}\int_0^{\infty}x^{u_{n_1}-u_{n_2}-1}\prod_{i=1}^{2}H_{1,1}^{1,1}\left[\frac{r^{\alpha_i}}{\varpi_i\hat{r}_i^{\alpha_i}x^{\alpha_i(i-1)}}\middle|\begin{matrix}(1-\mu_i-m_{s_i}-n_i,1)\\(0,1)\end{matrix}\right]dx. \tag{38}$$

$$\mathsf{E}[\Lambda^k]=\prod_{i=1}^{2}\frac{\Gamma\Big(\mu_i+\frac{k}{\alpha_i}\Big)\Gamma\Big(m_{s_i}-\frac{k}{\alpha_i}\Big)}{\Gamma(\mu_i)\Gamma(m_{s_i})}\left(\frac{p_i}{\zeta_i}\right)^{\vartheta_i}\varpi_i^{\frac{k}{\alpha_i}}\hat{r}_i\sum_{n_i=0}^{\infty}\frac{(\vartheta_i)_{n_i}\Big(\mu_i+\frac{k}{\alpha_i}\Big)_{n_i}}{(\mu_i)_{n_i}n_i!}\Big(-\varpi_i\Xi_i\Big)^{n_i}. \tag{40}$$

have

$$f_{Z_{E,\eta-\mathcal{F}}}(z)=\frac{(\mu\xi)^{\mu}[(m_s-1)\hat{r}^2]^{m_s}z^{\mu-1}}{B(\mu,m_s)[\mu\xi z+(m_s-1)\hat{r}^2]^{\mu+m_s}}\left(\frac{p}{\eta}\right)^{\vartheta}\times {}_2F_1\left(\vartheta,\mu+m_s;\mu;\frac{\mu\xi(\eta-p)z}{\eta[\mu\xi z+(m_s-1)\hat{r}^2]}\right), \tag{33}$$

where $\xi=(1+\eta)/(1+p)$, $\mu=(\mu_x+\mu_y)/2$, and $\hat{r}^2=\mathsf{E}[Z_{E,\eta-\mathcal{F}}]$.

The expression of $r$ under $\alpha$-$\eta$-$\mathcal{F}$ model is expressed as

$$r=\frac{\hat{r}R}{\sqrt{\mathsf{E}[R^2]}}=\frac{\hat{r}Z_{E,\eta-\mathcal{F}}^{\frac{1}{\alpha}}}{\sqrt{\mathsf{E}[Z_{E,\eta-\mathcal{F}}^{\frac{2}{\alpha}}]}}, \tag{34}$$

where $\mathsf{E}[Z_{E,\eta-\mathcal{F}}^{\frac{2}{\alpha}}]$ is the $\frac{2}{\alpha}$-th moment of the RV $Z_{E,\eta-\mathcal{F}}$ that is derived as [20, eq. (11)]

$$\mathsf{E}[Z_{E,\eta-\mathcal{F}}^{\frac{2}{\alpha}}]=\frac{B\Big(\mu+\frac{2}{\alpha},m_s-\frac{2}{\alpha}\Big){}_2F_1\Big(\vartheta,\mu+\frac{2}{\alpha};\mu;\frac{\eta-p}{\eta}\Big)}{B(\mu,m_s)\Big(\frac{(m_s-1)\hat{r}^2}{\mu\xi}\Big)^{-\frac{2}{\alpha}}\big(\frac{\eta}{p}\big)^{\vartheta}}. \tag{35}$$

Using (35) and the concept of the RVs transformation in

$$f_R(r)=\frac{\alpha r^{\alpha-1}}{\hat{r}^{\alpha}}\Big(\mathsf{E}\Big[Z_{E,\eta-\mathcal{F}}^{\frac{2}{\alpha}}\Big]\Big)^{\frac{\alpha}{2}}f_{Z_{E,\eta-\mathcal{F}}}\Big(\frac{r^{\alpha}}{\hat{r}^{\alpha}}\mathsf{E}\Big[Z_{E,\eta-\mathcal{F}}^{\frac{2}{\alpha}}\Big]^{\frac{\alpha}{2}}\Big). \tag{36}$$

Thereafter, performing some mathematical manipulations, (2) is yielded and this finishes the proof.

### B. Proof of Theorem 2

The PDF of the envelope of the product of two i.n.d. RVs, $\Lambda=R_1R_2$, can be computed by [31, eq. (3)]

$$f_{\Lambda}(r)=\int_0^{\infty}\frac{1}{x}f_{R_1}(x)f_{R_2}\left(\frac{r}{x}\right)dx. \tag{37}$$

Substituting (2) into (37) and invoking [18, eq. (1.2.4)] as well as [27, eq. (1.43)], we obtain (38) that is provided at the top of this page.

Using the identity [27, eq. (1.58)] and the substitution $u=x^{\alpha_2}$ in (38), the integral of (38) can be computed with the help of [27, eq. (2.3)]. Subsequently, doing some mathematical manipulations that include the using of [18, eqs. (1.1.5)/ (1.1.47)], the result is (4) and this ends the proof.

### C. Proof of Lemma 1

The expectation of the variate $\Lambda$ with power $k$ over $f_{\Lambda}(r)$ can be evaluated by

$$\mathsf{E}[\Lambda^k]=\int_0^{\infty}r^k f_{\Lambda}(r)dr. \tag{39}$$

Plugging (4) in (39) and employing $z=r^{\alpha_1}$ and [27, eq. (2.8)], the integral of (39) is calculated as in (40) given at the top of this page.

With the help of the definition [18, eq. (1.2.4)] and identity [18, eq. (1.1.47)], (6) is deduced and this ends the proof of Lemma 1.

### D. Proof of Lemma 2

The truncation error, $\varepsilon(M)$, via employing [32, eq. (25)]

$$\varepsilon(M)=\int_0^{\infty}\int_0^{\infty}(f(\gamma_B,\gamma_E)-\widehat{f}(\gamma_B,\gamma_E))d\gamma_B d\gamma_E, \tag{41}$$

where $\widehat{f}(\gamma_B,\gamma_E)$ is the truncated JPDF of (11) for $M$ terms that is obtained after using the identity [33, eq. (8.445)] for the function $I_a(.)$ as follows

$$\widehat{f}(\gamma_B,\gamma_E)=\frac{(1-\rho)^{a+1}}{4\Gamma(a+1)}\exp\left(-\left(\frac{\sqrt{\gamma_B}}{\Upsilon_B}+\frac{\sqrt{\gamma_E}}{\Upsilon_E}\right)\right)\times\sum_{n=0}^{M}\frac{\rho^n}{n!\Gamma(a+n+1)(\Upsilon_B\Upsilon_E)^{a+n+1}}(\gamma_B\gamma_E)^{\frac{a+n-1}{2}}. \tag{42}$$

Now, with the help of $\int_0^{\infty}\int_0^{\infty}f(\gamma_B,\gamma_E)d\gamma_B d\gamma_E=1$ [34, eq. (8)], the first double integrals of (42) is computed. The second double integral can be evaluated separately as two single integrals via invoking [33, eq. (3.478.1)] as follows

$$\int_0^{\infty}\gamma_l^{\frac{a+n-1}{2}}e^{-\frac{\sqrt{\gamma_l}}{\Upsilon_l}}d\gamma_l=2\Upsilon_l^{a+n+1}\Gamma(a+n+1), \tag{43}$$

where $l\in\{B,E\}$.

Finally, inserting the result of (43) and doing some mathematical simplifications via recalling the identity [33, eq. (1.1.15)], (12) is yielded and this concludes the proof.

## APPENDIX B

### A. Proof of Corollary 1

The ASC of (13) can be mathematically rewritten as [13, eq. (4)]

$$\bar{C}_s=\frac{1}{\ln(2)}(J_1-J_2), \tag{44}$$

This article has been accepted for publication in a future issue of this journal, but has not been fully edited. Content may change prior to final publication. Citation information: DOI: 10.1109/TVT.2026.3655009,



$$J_1 = \Psi \sum_{n=0}^{\infty} \frac{\rho^n \left(\frac{\Upsilon_B}{\Upsilon_E}\right)^{\psi_n}}{n!(a+1)_n} \frac{1}{(2\pi j)^2} \int_{\mathcal{S}} \int_{\mathcal{Z}} \frac{\Gamma(2\psi_n + 2s + z)\Gamma(1-s)\Gamma^2(s)\Gamma(-z)\Gamma(\psi_n + z)}{\Gamma(1+s)\Gamma(1+\psi_n+z)} \Upsilon_B^{2s} \left(\frac{\Upsilon_B}{\Upsilon_E}\right)^z dz ds. \tag{53}$$

$$J_2 = \Psi \sum_{n=0}^{\infty} \frac{\rho^n \left(\frac{\Upsilon_B}{\Upsilon_E}\right)^{\psi_n}}{n!(a+1)_n} \frac{1}{(2\pi j)^2} \int_{\mathcal{S}} \int_{\mathcal{Z}} \frac{\Gamma(2\psi_n + 2s + z)\Gamma(\psi_n + 2s + z)\Gamma(1-s)\Gamma^2(s)\Gamma(-z)}{\Gamma(1+\psi_n+2s+z)\Gamma(1+s)} \Upsilon_B^{2s} \left(\frac{\Upsilon_B}{\Upsilon_E}\right)^z dz ds. \tag{57}$$

where

$$J_1 = \int_0^{\infty} \int_0^{\gamma_B} \ln(1+\gamma_B) f(\gamma_B, \gamma_E) d\gamma_E d\gamma_B, \tag{45}$$

and

$$J_2 = \int_0^{\infty} \int_0^{\gamma_B} \ln(1+\gamma_E) f(\gamma_B, \gamma_E) d\gamma_E d\gamma_B. \tag{46}$$

To derive $J_1$, we firstly express $I_a(.)$ of (11) in terms of an infinite series via using [33, eq. (8.445)] and subsequently insert the result of $\gamma_E$ in (45). Thus, the following inner integral is yielded

$$J_{11} = \int_0^{\gamma_B} \gamma_E^{\frac{a+n-1}{2}} e^{-\frac{\sqrt{\gamma_E}}{\Upsilon_E}} d\gamma_E. \tag{47}$$

Re-expressing the exponential function of (47) in terms of the FHF via using [27, eq. (1.39)] and its definition that is provided in [27, eq. (1.2)] alongside with the change $x = \sqrt{\gamma_E}$, arrives the following result

$$J_{11} = \frac{1}{\pi j} \int_{\mathcal{Z}} \Gamma(-z) \Upsilon_E^{-z} \int_0^{\sqrt{\gamma_B}} x^{a+n+z} dx dz, \tag{48}$$

where $j = \sqrt{-1}$ and $\mathcal{Z}$ is the suitable contour in the $z$-plane from $\varrho - j\infty$ to $\varrho + j\infty$ with $\varrho$ is a constant value.

The linear integral of (48) can be readily calculated. Hence, with the aid of the property [18, eq. (1.1.5)], we have

$$J_{11} = \frac{\gamma_B^{\frac{a+n+1}{2}}}{\pi j} \int_{\mathcal{Z}} \frac{\Gamma(-z)\Gamma(a+n+1+z)}{\Gamma(a+n+2+z)} \left(\frac{\sqrt{\gamma}_B}{\Upsilon_E}\right)^z dz. \tag{49}$$

For the second integral of $J_1$, we substitute the terms of the variable $\gamma_B$ from the JPDF that is given in (11) and (49) into (45) to yield

$$J_{12} = \int_0^{\infty} \gamma_B^{a+n+\frac{z}{2}} \ln(1+\gamma_B) e^{-\frac{\sqrt{\gamma}_B}{\Upsilon_B}} d\gamma_B. \tag{50}$$

Replacing the natural logarithm function of (50) by the FHF via utilizing the identity [30, eq. (34)]. Then, after using the expansion principle for the FHF [27, eq. (1.2)], we obtains

$$J_{12} = \frac{1}{2\pi j} \int_{\mathcal{S}} \frac{\Gamma(1-s)\Gamma^2(s)}{\Gamma(1+s)} \int_0^{\infty} \gamma_B^{a+n+s+\frac{z}{2}} e^{-\frac{\sqrt{\gamma}_B}{\Upsilon_B}} d\gamma_B ds. \tag{51}$$

The inner integral of (51) is recorded in [33, eq. (3.478.1)]. Therefore, (51) becomes

$$J_{12} = \frac{\Upsilon_B^{2\psi_n}}{\pi j} \int_{\mathcal{S}} \frac{\Gamma(2\psi_n + 2s + z)\Gamma(1-s)\Gamma^2(s)}{\Gamma(1+s)} \Upsilon_B^{2s+z} ds. \tag{52}$$

Plugging $J_{11}$, $J_{12}$, and the remaining parts of (11) in (45) with some simple manipulations, $J_1$ is determined as in (53) shown at the top of this page.

Making use of [27, eq. (2.57)] for the double contour integrals of (53), $J_1'$ of (14) is deduced.

For $J_2$, we substitute the terms of $\gamma_E$ of (11) into (46) and utilize the variable representation $x = \sqrt{\gamma_E}$ alongside with the identities [30, eq. (34)] and [27, eq. (1.39)] to write the natural logarithm and exponential functions, respectively, in terms of a single FHF. Hence, by recalling [27, eq. (1.2)], we have

$$J_{21} = \frac{1}{(\sqrt{2}\pi j)^2} \int_{\mathcal{S}} \int_{\mathcal{Z}} \frac{\Gamma(1-s)\Gamma^2(s)\Gamma(-z)}{\Gamma(1+s)} \Upsilon_E^{-z} \times \int_0^{\sqrt{\gamma_B}} x^{\psi_n + 2s + z - 1} dx ds dz. \tag{54}$$

Evaluating the inner integral of (54) and invoking the identity [18, eq. (1.1.5)], the result is

$$J_{21} = \frac{1}{(\sqrt{2}\pi j)^2} \int_{\mathcal{S}} \int_{\mathcal{Z}} \frac{\Gamma(\psi_n + 2s + z)\Gamma(1-s)\Gamma^2(s)\Gamma(-z)}{\Gamma(1+\psi_n+2s+z)\Gamma(1+s)} \gamma_B^{\frac{\psi_n}{2}+s} \left(\frac{\sqrt{\gamma}_B}{\Upsilon_E}\right)^z ds dz. \tag{55}$$

Next, inserting the parts of $\gamma_B$ of (11) and (55) in (50), we have the following integral that is computed by [32, eq. (3.478.1)] as

$$J_{22} = \int_0^{\infty} \gamma_E^{\psi_n + s + \frac{z}{2} - 1} e^{-\frac{\sqrt{\gamma_B}}{\Upsilon_B}} d\gamma_B = \frac{2\Gamma(2\psi_n + 2s + z)}{\Upsilon_B^{-2\psi_n - 2s - z}}. \tag{56}$$

Substituting $J_{21}$ and $J_{22}$ as well as the terms of (11) that have not been employed in (54) and (56) into (46), we have $J_2$ as given in (57) presented at the top of this page.

With the assistance of the definition [27, eq. (2.57)], the integrals of (57) can be written in terms of the BFHF as in $J_2'$ of (14) which accomplishes the proof.

### B. Proof of Corollary 2

Making utilize of [33, eq. (8.445)] for (11) and inserting the result that includes the variate $\gamma_B$ in (18), the inner integral

can be computed with the help of [33, eq. (3.381.9)] as

$$I_1 = \int_{\theta\gamma_E+\theta-1}^{\infty} \gamma_B^{\frac{\psi_n}{2}-1} e^{-\frac{\sqrt{\gamma_B}}{\Upsilon_B}} d\gamma_B = \frac{2\Gamma\big(\psi_n, \frac{\sqrt{\theta\gamma_E+\theta-1}}{\Upsilon_B}\big)}{\Upsilon_B^{-\psi_n}}. \tag{58}$$

To calculate the outer integral of (18), we plug the terms of (11) and (58) that encompass $\gamma_E$. Therefore, this yields

$$I_2 = \int_0^{\infty} \gamma_E^{\frac{\psi_n}{2}-1} e^{-\frac{\sqrt{\gamma_E}}{\Upsilon_E}} \Gamma\left(\psi_n, \frac{\sqrt{\theta\gamma_E+\theta-1}}{\Upsilon_B}\right) d\gamma_E. \tag{59}$$

Now, applying the properties [27, eq. (1.39)] and [35, eq. (06.06.26.0005.01)] as well as introducing the definition of the FHF [27, eq. (1.2)] and interchanging the order of contour and linear integrals, (59) becomes

$$\begin{aligned} I_2 =& \frac{1}{(2\pi j)^2} \int_{\mathcal{S}} \int_{\mathcal{Z}} \frac{\Gamma(\psi_n - s)\Gamma(-s)\Gamma(-z)}{\Gamma(1-s)} \Upsilon_B^{-s} \Upsilon_E^{-z} \\ & \times \int_0^{\infty} \gamma_E^{\frac{\psi_n+z}{2}-1} (\sqrt{\theta\gamma_E+\theta-1})^s d\gamma_E dz ds. \end{aligned} \tag{60}$$

Computing the linear integral of (60) via using [33, eq. (3.194.3)]. Afterward, recalling [18, eq. (1.1.47)], we obtain

$$\begin{aligned} I_2 =& \frac{\big(1-\frac{1}{\theta}\big)^{\frac{\psi_n}{2}}}{(2\pi j)^2} \int_{\mathcal{S}} \int_{\mathcal{Z}} \frac{\Gamma\big(-\frac{\psi_n+s+z}{2}\big)\Gamma(\psi_n - s)\Gamma(-s)}{\Gamma(1-s)\Gamma(-\frac{s}{2})} \\ & \times \Gamma(-z)\Gamma\Big(\frac{\psi_n+z}{2}\Big)\left(\frac{\sqrt{\theta-1}}{\Upsilon_B}\right)^s \left(\frac{\sqrt{\theta-1}}{\theta\Upsilon_E}\right)^z dz ds. \end{aligned} \tag{61}$$

Substituting the term $2\Upsilon_B^{\psi_n}$ of (58) and $I_2$ of (61) alongside with the parts of (11) that have not been used in (58) and (59), the result in (19) is concluded after recognizing the definition of the BFHF [27, eq. (2.57)] which completes the proof.

### C. Proof of Corollary 3

Comparing the inner integral of the $P_c^L$ in (21) with (58), one can obtain the following expression

$$I_1^L = 2\Upsilon_B^{\psi_n} \Gamma\left(\psi_n, \frac{\sqrt{\theta\gamma_E}}{\Upsilon_B}\right). \tag{62}$$

Based on (61), the outer integral of (21) can be deduced from (59) after omitting the term $\theta - 1$. Next, making employ of [35, eq. (06.06.26.0005.01)] and [27, eq. (1.2)] for the upper incomplete Gamma function, we have

$$\begin{aligned} I_2^L =& \frac{1}{2\pi j} \int_{\mathcal{S}} \frac{\Gamma(\psi_n - s)\Gamma(-s)}{\Gamma(1-s)} \left(\frac{\sqrt{\theta}}{\Upsilon_B}\right)^s \\ & \times \int_0^{\infty} \gamma_E^{\frac{\psi_n+s}{2}-1} e^{-\frac{\sqrt{\gamma_E}}{\Upsilon_E}} d\gamma_E ds. \end{aligned} \tag{63}$$

Invoking [33, eq. (3.478.1)] to evaluate the integral of (63), $I_2^L$ is expressed as

$$I_2^L = \frac{\Upsilon_E}{\pi j} \int_{\mathcal{S}} \frac{\Gamma(\psi_n + s)\Gamma(\psi_n - s)\Gamma(-s)}{\Gamma(1-s)} \left(\frac{\sqrt{\theta}\Upsilon_E}{\Upsilon_B}\right)^s. \tag{64}$$

Using [18, eq. (1.5.15] for (64) and inserting the result alongside with (62) as well as the remaining terms of (11) in (21), the expression of the $P_c^L$ that is provided in (22) is derived which accomplishes the proof.

## APPENDIX C

### A. Proof of Corollary 4

The expression of the ASC at high $\gamma_B$ and $\gamma_E$ depends on the asymptotic of $J_1'$ and $J_2'$, namely, $J_1'^{\text{Asy}}$ and $J_2'^{\text{Asy}}$, respectively. However, both $J_1'$ and $J_2'$ are included the BFHF that can be expressed in terms of double contour integrals as shown in (53) and (57). Consequently, with the help of the residue theorem that was extensively used in [36], the closed-form expressions of $J_1'^{\text{Asy}}$ and $J_2'^{\text{Asy}}$ are derived.

According to the residue approach, when $\bar{\gamma}_B \to \infty$, namely, $\Upsilon_B \to \infty$, the highest poles on the left of $\mathcal{S}$ of (53) which occur at $s = -\psi_n - \frac{z}{2}$ and $s = 0$ can be calculated as

$$\begin{aligned} \mathbf{S} =& \frac{1}{2\pi j} \int_{\mathcal{S}} \frac{\Gamma(2\psi_n + 2s + z)\Gamma(1-s)\Gamma^2(s)}{\Gamma(1+s)} \Upsilon_B^{2s} ds \\ =& \operatorname{Res}\left[\frac{\Gamma(1-s)\Gamma^2(s)\Upsilon_B^{2s}}{\Gamma(1+s)}, -\psi_n - \frac{z}{2}\right] \\ &+ \operatorname{Res}\left[\frac{\Gamma(2\psi_n + 2s + z)\Gamma(1-s)}{\Gamma(1+s)} \Upsilon_B^{2s}, 0\right] \\ =& \frac{\Gamma\big(1+\psi_n+\frac{z}{2}\big)\Gamma^2\big(-\psi_n-\frac{z}{2}\big)}{\Gamma\big(1-\psi_n-\frac{z}{2}\big)\Upsilon_B^{2\psi_n+z}} + \Gamma(2\psi_n + z). \end{aligned} \tag{65}$$

Next, substituting the result of (65) into (53), the following two contour integrals are obtained

$$\begin{aligned} \mathbf{Z} =& \frac{1}{\Upsilon_B^{2\psi_n}} \\ & \frac{1}{2\pi j} \int_{\mathcal{Z}} \frac{\Gamma\big(1+\psi_n+\frac{z}{2}\big)\Gamma^2\big(-\psi_n-\frac{z}{2}\big)\Gamma(-z)\Gamma(\psi_n+z)}{\Gamma\big(1-\psi_n-\frac{z}{2}\big)\Gamma(1+\psi_n+z)\Upsilon_E^z} dz \\ & + \frac{1}{2\pi j} \int_{\mathcal{Z}} \frac{\Gamma(2\psi_n+z)\Gamma(-z)\Gamma(\psi_n+z)}{\Gamma(1+\psi_n+z)} \left(\frac{\Upsilon_B}{\Upsilon_E}\right)^z dz. \end{aligned} \tag{66}$$

At high $\bar{\gamma}_B$, the most prominent pole on the right side of the contour integral $\mathcal{Z}$ of the second term of (66) is obtained at $z = -\psi_n$. Therefore, applying the residue method for the second contour integral, we have

$$\begin{aligned} \mathbf{Z} =& \Gamma^2(\psi_n)\left(\frac{\Upsilon_E}{\Upsilon_B}\right)^{\psi_n} + \frac{1}{\Upsilon_B^{2\psi_n}} \\ & \frac{1}{2\pi j} \int_{\mathcal{Z}} \frac{\Gamma\big(1+\psi_n+\frac{z}{2}\big)\Gamma^2\big(-\psi_n-\frac{z}{2}\big)\Gamma(-z)\Gamma(\psi_n+z)}{\Gamma\big(1-\psi_n-\frac{z}{2}\big)\Gamma(1+\psi_n+z)\Upsilon_E^z} dz. \end{aligned} \tag{67}$$

When $\bar{\gamma}_E$ becomes high, (67) can be further approximated via using the residue approach at $z = 0$ and $z = -2\psi_n$ and recalling the property [18, eq. (1.1.6)]. Hence, $J_1'^{\text{Asy}}$ that is given in (25) is deduced.

Following the analogous methodology that is used for $J_1'^{\text{Asy}}$, the expression of $J_2'^{\text{Asy}}$ at $\Upsilon_B \to \infty$ can be derived by first computing the highest poles of $\mathcal{S}$ of (57) at $s = 0$ and $s = -\frac{\psi_n+z}{2}$. Thereafter, calculating the result at pole of the right side of $\mathcal{Z}$, i.e., $z = -\psi_n$, this yields

$$\begin{aligned} \mathbf{Z} =& \Gamma^2(\psi_n)\left(\frac{\Upsilon_E}{\Upsilon_B}\right)^{\psi_n} + \frac{\Gamma(\psi_n)}{\Upsilon_B^{\psi_n}} \\ & \frac{1}{2\pi j} \int_{\mathcal{Z}} \frac{\Gamma^2\big(-\frac{\psi_n+z}{2}\big)\Gamma\big(-z\big)\Gamma(1+\frac{\psi_n}{2}+z)}{\Gamma\big(1-\frac{\psi_n+z}{2}\big)\Upsilon_E^z} dz. \end{aligned} \tag{68}$$

This article has been accepted for publication in a future issue of this journal, but has not been fully edited. Content may change prior to final publication.
Citation information: DOI: 10.1109/TVT.2026.3655009,



Similar to (67), when $\bar{\gamma}_E \to \infty$, the residue theorem can be applied for the contour integral of (68) at $z = 0$ and $z = -\psi_n$. Accordingly, $J_2'^{\text{Asy}}$ that is provided in (26) is straightforwardly obtained which achieves the proof.

### B. Proof of Corollary 5

When $\bar{\gamma}_B$ tends to infinity, namely, $\Upsilon_B \to \infty$, the highest poles of $\mathcal{S}$ of (61) can be computed at $s = \psi_n$ and $s = 0$ via utilizing the residue theorem. Thus, this yields

$$\mathbf{S} = \frac{\Gamma\big(-\frac{2\psi_n+z}{2}\big)\Gamma(-\psi_n)}{\Gamma(1-\psi_n)\Gamma(-\frac{\psi_n}{2})}\left(\frac{\sqrt{\theta-1}}{\Upsilon_B}\right)^{\psi_n} + \Gamma(\psi_n)\Gamma\Big(-\frac{\psi_n+z}{2}\Big). \tag{69}$$

Plugging (69) in (61), leads to the following result

$$I_2^{\text{Asy}} = \frac{\big(1-\frac{1}{\theta}\big)^{\frac{\psi_n}{2}}}{2\pi j}\int_{\mathcal{Z}}\left(\frac{\sqrt{\theta-1}}{\theta\Upsilon_E}\right)^{z}\Bigg\{\left(\frac{\sqrt{\theta-1}}{\Upsilon_B}\right)^{\psi_n} \frac{\Gamma(-\psi_n)}{\Gamma(1-\psi_n)\Gamma(-\frac{\psi_n}{2})}\Gamma\Big(-\frac{2\psi_n+z}{2}\Big)\Gamma(-z)\Gamma\Big(\frac{\psi_n+z}{2}\Big) + \Gamma(\psi_n)\Gamma\Big(-\frac{\psi_n+z}{2}\Big)\Gamma(-z)\Gamma\Big(\frac{\psi_n+z}{2}\Big)\Bigg\}dz. \tag{70}$$

For $\bar{\gamma}_E$ approaches infinity, the residue method can be used for (70) via substituting $z = 0$ and $z = -\psi_n$. Now, following the same steps that are utilized in Appendix C.A, the proof of (27) is accomplished.

### C. Proof of Corollary 6

The asymptotic of (22) when $\bar{\gamma}_B$ goes to infinity can be derived via recalling the residue approach to evaluate the highest poles of $\mathcal{S}$ of (64) at $s = \psi_n$ and $s = 0$. Subsequently, using the same procedure that is followed for (64) of Appendix B.C, the result is (28) and this completes the proof.

## REFERENCES

[1] S. Basharat *et al.*, "Reconfigurable intelligent surfaces: Potentials, applications, and challenges for 6G wireless networks," *IEEE Wireless Commun.*, vol. 28, no. 6, pp. 184-191, Dec. 2021.

[2] W. Shi, W. Xu, X. You, C. Zhao, and K. Wei, "Intelligent reflection enabling technologies for integrated and green internet-of-everything beyond 5G: Communication, sensing, and security," *IEEE Wireless Commun.*, vol. 30, no. 2, pp. 147-154, Apr. 2023.

[3] L. Yang *et al.*, "Secrecy performance analysis of RIS-aided wireless communication systems," *IEEE Trans. Veh. Technol.*, vol. 69, no. 10, pp. 12296-12300, Oct. 2020.

[4] Y. Ai *et al.*, "Secure vehicular communications through reconfigurable intelligent surfaces," *IEEE Trans. Veh. Technol.*, vol. 70, no. 7, pp. 7272-7276, July 2021.

[5] A. K. Yadav *et al.*, "Secrecy performance analysis of RIS-enabled wireless networks over Rayleigh fading channels," in *Proc. IEEE Advanced Commun. Technol. Sig. Proc. (ACTS)*, Dec. 2021, pp. 1-6.

[6] A. K. Yadav, S. Yadav, A. Pandey, and Adão Silva, "On the secrecy performance of RIS-enabled wireless communications over Nakagami-$m$ fading channels," *ICT Express*, vol. 9, no. 3, pp. 452-458, June 2023.

[7] I. Trigui, W. Ajib, and W.-P. Zhu, "Secrecy outage probability and average rate of RIS-Aided communications using quantized phases," *IEEE Commun. Lett.*, vol. 25, no. 6, pp. 1820-1824, June 2021.

[8] W. Shi *et al.*, "On secrecy performance of RIS-assisted MISO systems over Rician channels with spatially random eavesdroppers," *IEEE Trans. Wireless Commun.*, vol. 23, no. 8, pp. 8357-8371, Aug. 2024.

[9] F. R. Ghadi, W. P. Zhu, and D.Martín, "RIS-aided secure communications over Fisher-Snedecor $\mathcal{F}$ fading channels," Apr. 2023, *arXiv:2208.07274*.

[10] S. Pakravan *et al.*, "Physical-layer security of RIS-assisted networks over correlated Fisher-Snedecor $\mathcal{F}$ fading channels," *IEEE J. Internet of Things*, vol. 11, no. 9, pp. 15152-15165, May 2024.

[11] J. Zhang *et al.*, "Physical layer security enhancement with reconfigurable intelligent surface-aided networks," *IEEE Trans. Info. Forensics Security*, vol. 16, pp. 3480-3495, May 2021.

[12] A.A. A. Boulogeorgos, A. Alexiou, and A. Michalas, " On the physical layer security capabilities of reconfigurable intelligent surface empowered wireless systems," Aug. 2023, *https://arxiv.org/abs/2308.09906*

[13] A. Mathur, Y. Ai, M. Cheffena and G. Kaddoum, "Secrecy performance of correlated $\alpha$-$\mu$ fading channels," *IEEE Communi. Lett.*, vol. 23, no. 8, pp. 1323-1327, Aug. 2019.

[14] A. I. Perez-Neira *et al.*, "Signal processing for high-throughput satellites: Challenges in new interference-limited scenarios," *IEEE Sig. Proc. Mag.*, vol. 36, no. 4, pp. 112-131, 2019.

[15] O. S. Badarneh, "The $\alpha$-$\eta$-$\mathcal{F}$ and $\alpha$-$\kappa$-$\mathcal{F}$ composite fading distributions," *IEEE Commun. Lett.*, vol. 24, no. 9, pp. 1924-1928, Sept. 2020.

[16] H. Silva *et al.*, "The extended $\eta$-$\mathcal{F}$ composite fading distribution," *IEEE Trans. Veh. Technol.*, vol. 71, no. 9, pp. 10104 - 10109, Aug. 2022.

[17] G. R. d. L. Tejerina *et al.*, "On the extended $\eta-\mu$ model: New results and applications to IRS-aided systems," *IEEE Trans. Veh. Technol.*, vol. 72, no. 4, pp. 4133-4142, Apr. 2023.

[18] H. M. Srivastava, and H. L. Manocha, *A Treatise on Generating Functions*, Wiley, New York, 1984.

[19] S. K. Yoo *et al.*, "The $\kappa$-$\mu$/inverse gamma and $\eta$-$\mu$/inverse gamma composite fading models: fundamental statistics and empirical validation," *IEEE Trans. Commun.*, vol. 69, no. 8, pp. 5514-5530, Aug. 2021.

[20] S. K. Yoo *et al.*, "The Fisher-Snedecor $\mathcal{F}$ distribution: A simple and accurate composite fading model," *IEEE Commun. Lett.*, vol. 21, no. 7, pp. 1661-1664, July 2017.

[21] G. R. de Lima Tejerina *et al.*, "Extended $\eta$-$\mu$ fading models," *IEEE Trans. Wireless Commun.*, vol. 19, no. 12, pp. 8153-8164, Dec. 2020.

[22] O. S. Badarneh, "The $\alpha$-$\mathcal{F}$ composite fading distribution: Statistical characterization and applications," *IEEE Trans. Veh. Technol.*, vol. 69, no. 8, pp. 8097-8106, Aug. 2020.

[23] H. Al-Hmood, R. S. Abbas, and H. Al-Raweshidy, "Extended $\alpha$-$\eta$-$\mu$ fading distribution: Statistical properties and applications," *IEEE Access*, vol. 10, 109803-109813, Oct. 2022.

[24] S. Primak, V. Kontorovich, and V. Lyandres, *Stochastic methods and their applications to communications: stochastic differential equations approach*, John & Wiley Sons, 2005.

[25] M. D. Yacoub, "The $\alpha$-$\mu$ distribution: A physical fading model for the stacy distribution," *IEEE Trans. Veh. Technol.* vol. 56, no. 1, pp. 27-34, Jan. 2007.

[26] F. R. Ghadi and G. A. Hodtani, "Copula-based analysis of physical layer security performances over correlated Rayleigh fading channels," *IEEE Trans. Info. Forensics Security*, vol. 16, pp. 431-440, Aug. 2021.

[27] A. M. Mathai, R. K. Saxena, and H. J. Haubold, *The $H$-function: Theory and applications*, 1st ed. New York, NY, USA: Springer, 2009.

[28] M. M. Rahman *et al.*, "RIS-aided mixed RF-FSO wireless networks: Secrecy performance analysis with simultaneous eavesdropping," *IEEE Access*, vol. 11, pp. 126507-126523, 2023.

[29] H. Chergui, M. Benjillali, and M.-S. Alouini, *GPU-Enabled Multivariate Fox H-Function Code*, Zenodo, Geneva, Switzerland, Aug. 2018, https://zenodo.org/records/1400403.

[30] H. Al-Hmood and H. Al-Raweshidy, "Performance analysis of physical layer security over fluctuating Beckmann fading channels," *IEEE Access*, vol. 7, pp. 119541-119556, Aug. 2019.

[31] H. Al-Hmood and H. S. Al-Raweshidy,, "Unified composite distribution with applications to double shadowed $\kappa$-$\mu$ fading channels," *IEEE Trans. Veh. Technol.*, vol. 70, no. 7, pp. 7182-7186, July 2021.

[32] H. Al-Hmood and H. S. Al-Raweshidy, "On the effective rate and energy detection based spectrum sensing over $\alpha$-$\eta$-$\kappa$-$\mu$ fading channels," *IEEE Trans. Veh. Technol.*, vol. 69, no. 8, pp. 9112-9116, Aug. 2020.

[33] I. S. Gradshteyn, and I. M. Ryzhik, *Table of Integrals, Series and Products*, 7th edition. Academic Press Inc., 2007.

[34] I. Trigui, A. Laourine, S. Affes, and A. Stéphenne, "Bivariate $\mathcal{G}$ distribution with arbitrary fading parameters," *Int. Conf. Sign., Circuits and Systems (SCS)*, Medenine, Tunisia, Nov. 2009, pp. 1-5.

[35] "The Wolfram Functions Website" http://functions.wolfram.com.

[36] L. Kong, "Wireless networks physical layer security: modeling and performance characterization." Ph.D. dissertation, École de Technologie Supérieure, Aug. 2019.